Mechanical Effects of Lubrication on Nanoscratching by Molecular Dynamics Simulations

S. Stephan,[1, a)] M. P. Lautenschlaeger,[1] I. Alabd Alhafez,[2] M. T. Horsch,[1] H. M. Urbassek,[2] and H. Hasse[1]
[1)] *Laboratory of Engineering Thermodynamics (LTD), University of Kaiserslautern, 67663 Kaiserslautern, Germany*
[2)] *Physics Department and Research Center OPTIMAS, University of Kaiserslautern, 67663 Kaiserslautern, Germany*

(Dated: 10 August 2017)

Friction, wear and adhesion play a dominant role in many technical processes, such as machining by cutting and grinding. We conduct fully atomistic simulations of a tribological contact process (indentation, scratching and retraction) and compare three different cases: one dry reference case and two lubricated cases differing in the solid-fluid adsorption energy. The fluid as the substrate is modelled as a bulk phase, to determine the bulk phase reaction as well as the interfacial mechanisms. We investigate the influence of the lubrication fluid on the mechanical properties of the contact process, e. g. the friction forces, the coefficient of friction, the squeeze-out of fluid molecules from the contact zone and characterize the groove, the chip and the lubrication gap formation during the simulation. We observe, that the presence of a fluid and its solid-fluid adsorption energy has a significant influence on the contact process, e. g. the friction forces and the squeeze-out.

Keywords: Nanotribology, single asperity contact, molecular dynamics, squeeze-out

I. INTRODUCTION

Friction and machining processes on atomistic scale are yet not fully understood, although this research area has been worked on for decades. While many aspects of dry nanoscopic contact processes have been investigated in great detail by experimental, theoretical[1,2] and simulation techniques[3–8], lubricated processes are less extensively studied in literature. Dry nanoindentation, -scratching, cutting and machining processes[9,10] have been studied in great detail with different focus, for example the influence of the shape of the tool[11,12], different substrate materials[3,13,14], the indentation depth[13], the cutting direction in relation to the lattice orientation[15], the influence of the temperature, grain boundaries[16], the surface roughness[17], alloys[18] and coatings[19].

Lubricated contact processes are the subject of many studies in the last decade[20–23]. Questions like the influence of crafted polymer brushes on a substrate in tribological systems[24,25], the influence of the chain length[26,27] of a lubricant and in combination with the surface roughness[28] or the influence of monolayer or multilayer adsorbates[29–38] have been investigated in the last years. Also the bridging from experimental measurements to atomistic simulation results has been successful to some extent[39–42]. But many open questions in the field of lubricated nano-friction remain, for example the influence of the surface chemistry[43], the solid-fluid interaction on the squeeze-out[28,44], the influence of the fluid on the chip formation and the influence of a lubricant on the thermal balance of the contact process. Furthermore, in most studies investigating a single asperity contact under the influence of a lubricant, only mono- or multilayer fluids are taken into account. A bulk fluid phase, having a solid-liquid interface with the substrate and the tool, is only rarely investigated[45–47]. Often, either the fluid or the substrate is modelled as a monoatomic layer, while interfacial properties and processes are taken into account. But crossinteractions resulting from modelling the bulk phase of the substrate (e. g. dislocation analysis) and the bulk phase of the fluid and interfacial properties are to the best of our knowledge not yet systematically investigated.

In the present study, we investigate the influence of a monoatomic fluid on the mechanical properties, such as the coefficient of friction (COF), dislocations and friction forces, of a nano-indentation, -scratching and -retraction process. We therefore compare a dry contact process with two different lubricated cases. A special focus lies on the squeeze-out of the fluid, which is in contrast to other studies not modelled as a very thin adsorbed layer in the contact zone without a surrounding bulk fluid phase and the dislocation analysis. Therefore, the entire simulation box is in the present study filled with liquid in the lubricated cases, confined in a constant volume. Also we study the influence of the adsorption interaction of fluid molecules with solid atoms on the above mentioned mechanical properties. *Becker et al.*[48] showed, that the adsorption energy correlates with the wetting state, e. g. the contact angle formed between a liquid droplet on a solid surface. The fluid and the substrate have a bulk phase to realistically model the interaction between the contact zone, the interfaces and the bulk phases.

The target of the present study lies in the investigation of the influence of a lubrication fluid on the mechanical properties in an atomistic contact process and the characterization of the contact zone. We address the question how long and how many fluid particles remain in the lubrication gap during an atomistic friction process and how this squeeze-out depends on the adsorption

[a)] corresponding author: simon.stephan@mv.uni-kl.de

energy. We analyse the influence of the presence of a lubrication fluid and its adsorption energy on the friction forces, the coefficient of friction (COF) and the dislocation behaviour in the substrate. Moreover it is shown, that the modelling of the fluid bulk phase has a considerable influence on the chip formation and the machined surface quality.

The article is organised in two main sections: in the first section *methods* we introduce the simulation scenario and potential models and define characteristic properties for the contact process regarding the squeeze-out, chip formation and machined surface. In the *result* section we compare the results of the three simulations (dry, strong and weak adsorption).

II. METHODS

A. Simulation Setup

We employ molecular dynamics simulation to study the difference of a dry and wet nano-scratching contact. Fig. 1 shows the simulation setup. The so-called indenter models the edge of a diamond AFM tip. The indenter (purple) conducts three sequential movements to model the nanoscopic contact: (i) indention, during which the indenter penetrates into the substrate (yellow) in normal direction; (ii) the indenter moves laterally to the substrate during the scratching phase and grooves it; (iii) the indenter is finally removed from the contact during the retraction phase until no interaction between the substrate and the indenter remains. The coordinate system, as indicated in Fig. 1, has its origin $z = 0$ on the unpenetrated surface of the substrate. The indentation and retraction movement is aligned with the z-axis.

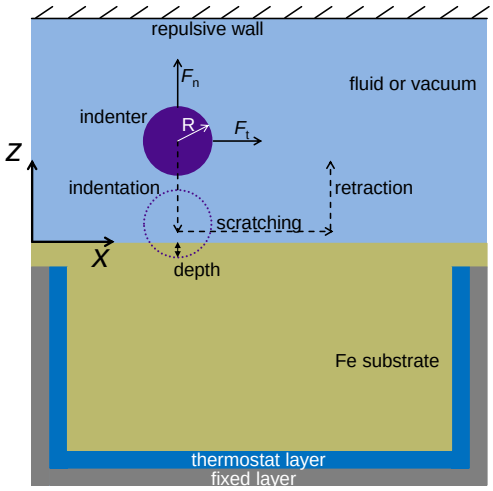

FIG. 1. Setup of the simulation box for the indentation, scratching and retracting of the indenter. The indenter is either in a vacuum environment (dry case) or immersed in fluid (two lubricated cases).

The scratching is conducted in positive x-direction. The simulation box has periodic boundary conditions in x- and y-direction, while we adopt a repulsive wall boundary condition at the top and bottom of the box in z-direction. In the dry simulation the surrounding of the indenter is vacuum, while the indenter is submersed with fluid in the lubricated case. All three simulations have an initial temperature of 100 K.

The indenter has a spherical shape with a radius of $R = 5\,\text{nm}$ and is atomically resolved in contrast to former studies of our group[3]. This is done to ensure appropriate stick-slip behaviour and squeeze-out of the fluid, especially to investigate the influence of the adsorption energy on those phenomena. The diamond indenter is modelled as one rigid body, e. g. the relative distances of all carbon atoms to each other remain constant throughout the simulation. In fact, we prescribe the velocities of the carbon atoms according to the above mentioned movement phases of the indenter. The simplification of a rigid indenter is based on the large hardness difference of diamond (10 on *Mohs-scale*) and iron (4.0 on *Mohs-scale*). The indenter consists of appr. 92 thousand atoms. The indenter atoms interact purely repulsive with the substrate by a Lennard-Jones potential[49], as done in many other studies[11,15,16] . The indentation depth is set constant in all three simulations to 3 nm.

The substrate is a bcc iron single crystal. It has initially an atomically flat surface. It is modelled with the iron embedded atom model (EAM) from *Mendelev et al.*[50]. The crystal has a (100) surface; we scratch in [0 $\bar{1}$ $\bar{1}$] direction. The size of the substrate block is 52.5 nm; 62.6 nm; 27.2 nm in x-, y- and z-direction respectively and consists of appr. 7.7 million Fe atoms. This relatively large substrate size is chosen to avoid any interaction of the generated dislocations with the boundaries. Three atom layers of the substrate block boundary (grey) have a fixed position to suppress a movement of the substrate block relative to the coordinate system of the simulation box. Four more atom layers(dark blue) are being time-integrated, but their trajectories are perturbed by a velocity scaling thermostat to extract dissipated energy from the system to avoid an uncontrolled heating up. To preclude any interaction of the fluid with the thermostat and the fixed layer of the substrate, a lid of 'regular' iron atoms is placed on the substrate block. The initial temperature of 100 K is imposed to the thermostat-layer during the entire simulation sequence.

Methane is used as a liquid lubricant which is modelled in a united atom approach[51], e. g. the hydrogen atoms are not explicitly resolved. The spherically shaped CH_4 molecule is therefore modelled by a single Lennard-Jones 12-6 interaction site. A cutoff distance of $2.5\,\sigma_\text{F} = 9.31\,\text{Å}$ until interactions are taken into account is employed to avoid time-consuming long-range correction schemes[52]. We use the parameters proposed by *Vrabec et al.* ($\varepsilon_\text{F} = 0.0151\,\text{eV/Å}$ and $\sigma_\text{F} = 3.7241\,\text{Å}$), who showed that the model reproduces the fluid bulk properties of methane quite accurately[53]. The fluid is

being enclosed in a constant volume by the substrate surface and a soft repulsive wall on top of the simulation box. Thereby it experiences a isochoric state change during the simulation. The fluid has a density of $0.4389\,\mathrm{g/cm^3}$ and an initial pressure of 1.1 bar. At this density and temperature the fluid (force field model and measurement data[53,54]) is in the state of a subcooled liquid. The position of the soft repulsive wall is at $z_{\mathrm{wall}} = 28.2\,\mathrm{nm}$ and encloses 1.5 million methane molecules.

The contact angle and therefore the wetting behaviour of a fluid is of great importance for many engineering applications. For the investigation of the influence of the adsorption energy $\varepsilon_{\mathrm{solid\text{-}fluid}}$ of fluid molecules on the solid in a atomistic friction process, we conduct two lubricated simulations only differing in this energy parameter. It was shown by *Becker et al.*[48], that the adsorption energy of monoatomic particles correlates directly with the contact angle. In some simulation studies for the investigation of lubricated contact processes the solid-fluid interaction energy is set accordingly to quantum mechanical calculations or experimental spectroscopic measurements. This is based on the assumption, that the contact zone is by no means contaminated, which we know from many studies is not accurate for technical surfaces[55,56]. We therefore argue, that an investigation of the influence of the wetting behaviour of a fluid on a tribological system should be independently conducted from the fluid-substrate combination and it's chemistry. We hence study in the present work two different wetting states: a weak adsorption case with a solid-fluid interaction energy of $\varepsilon_{\mathrm{weak\text{-}ads.}} = 0.00503\,\mathrm{eV/Å}$ resulting in a lower contact angle than a strong adsorption case with $\varepsilon_{\mathrm{strong\text{-}ads.}} = 0.01723\,\mathrm{eV/Å}$. The solid-fluid interaction between the fluid and the indenter and the fluid and the substrate were modelled the same in each of the two lubricated simulations. As done in most studies, we apply the Lennard-Jones 12-6 potential for the adsorption interaction. Its size parameter $\sigma_{\mathrm{ads.}}$ is set to the same as the size parameter of the methane model $\sigma_{\mathrm{CH_4}}$.

Before the sequential move of the indenter the system is equilibrated for 1000 ps. The timestep during the equilibration and the production phase is kept constant at 0.001 ps. The indenter moves with a constant velocity of 20 m/s during all three movement phases (i)-(iii). First in negative z-direction for 300 ps ($\Delta z = -6\,\mathrm{nm}$), followed by the scratching in x-direction for 400 ps ($\Delta x = 8\,\mathrm{nm}$) and the retraction of the indenter for 175 ps ($\Delta z = 3.5\,\mathrm{nm}$). The time axis plotted throughout this paper has its origin at the starting point of the indenter movement.

The simulations were performed with the open-source code LAMMPS[57]. The dislocation extraction algorithm (DXA)[58] is used to identify the dislocations, to determine their Burgers vectors, and to measure the total length of the dislocation lines, Ldisl. The free software tools ParaView[59], visit[60] and OVITO[61] are employed to visualize the atomistic configurations.

B. Characterization of the Contact Process

For the mechanical evaluation and comparison of the three simulations, we adapt multiple post-processing schemes. We examine the forces on the indenter, the COF, the dislocation behaviour in the substrate, the chip formation and the squeeze-out of fluid molecules out of the contact zone in the lubricated simulations. Also we discuss the machined surface in the groove, since the surface quality is an important aspect in manufacturing processes, such as grinding[62]. In this section we define the characteristic values for the evaluation of the named properties.

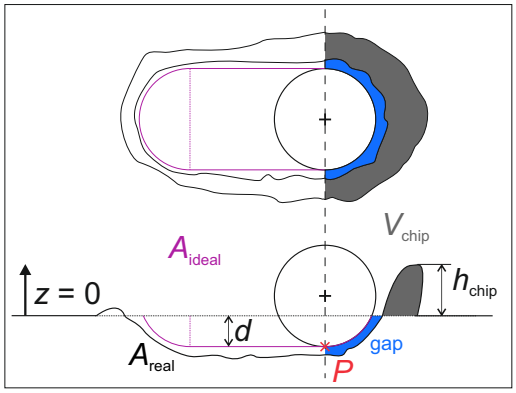

FIG. 2. Geometric definition of the lubrication gap (blue) for the calculation of its volume and the fluid particles in it and the geometric definition of the surface quality parameter used in this work. Also we characterize the machined chip by its volume and hight.

For the calculation of the mainly geometrically defined properties, we use an alpha-shape algorithm[63] to calculate the surface area of the machined substrate every 30 ps. It calculates the surface of the indenter and the penetrated substrate by identifying the atoms forming the actual surface and connecting them to k triangles $A_k^{\alpha}(x, y, z)$.

Friction Forces:

The friction forces and thereby the COF are calculated by the total force on the indenter in x- and z-direction, the tangential force F_{t} and the normal force F_{n} respectively. They are evaluated during the simulation as the sum of all pair interactions m in the cut-off radius $F_i^{\mathrm{Ind\text{-}Subs}}$ between indenter and substrate atoms on one side and indenter and fluid atoms on the other side $F_i^{\mathrm{Ind\text{-}Fluid}}$:

$$F_{\mathrm{t}} = \sum_{i=1}^{m} \left(F_{\mathrm{t}.i}^{\mathrm{Ind\text{-}Subs}} + F_{\mathrm{t}.i}^{\mathrm{Ind\text{-}Fluid}} \right) \tag{1}$$

$$F_{\mathrm{n}} = \sum_{i=1}^{m} \left(F_{\mathrm{n}.i}^{\mathrm{Ind\text{-}Subs}} + F_{\mathrm{n}.i}^{\mathrm{Ind\text{-}Fluid}} \right) \tag{2}$$

The COF is then calculated by $\mu = F_{\mathrm{t}}/F_{\mathrm{n}}$.

Dislocation Analysis:
During indentation and scratching extended lattice defects are formed in the crystal; these consist of dislocations. The analysis of the dislocations formed thus allows us to gain insight into the reaction of the iron crystal to the machining process, and to what extent it is influenced by the lubrication.

Characterization of Contact Zone:
We define the contact zone of the indenter and the substrate as the area where the indenter is in touch with the unmachined substrate, as indicated in Fig. 2. This contact can either be dry (no fluid particles in-between the indenter and the substrate) or lubricated (fluid particles trapped in the gap). We therefore calculate the gap volume in all three cases and the number of fluid molecules trapped in there for both lubricated simulations.

We use the surfaces elements $A_k^\alpha(x, y, z)$ calculated with the alpha-shape algorithm for the evaluation of the gap volume. It is evaluated by subtracting the volume under the substrate surface from the volume under the indenter surface of the contact zone (highlighted blue in fig. 2). By knowing the gap volume and its coordinates, it is straight forward to count the trapped fluid particles in the gap.

Quality of Machined Surface:
A high surface quality goes in line with a low surface roughness. It is well known from experience[64], that the presence of a lubricant decreases the machined surface roughness significantly. We therefore define a so-called *surface enlargement* $A_{\text{real}}/A_{\text{ideal}}$, which is a measure for the increase of the machined surface due to an increased atomistic roughness. The ideal surface A_{ideal} is calculated (eq. (3)) from the assumption of a perfect spherical indenter and an ideal impress (indicated purple in fig. 2).

$$A_{\text{ideal}} = 2\left(2\pi R d + 2x_{\text{P}} R \arccos\left(\frac{R-d}{R}\right)\right), \quad (3)$$

where R is the indenter radius, d the indentation depth and x_{P} is the position of the indenter. The substrate surface elements in the groove – gained from the alpha-shape algorithm – are summed up to A_{real}, where the groove is defined as the projection of the ideal shape of the groove.

$$A_{\text{real}} = \sum A^\alpha_{\text{Subs}.k}(x, y) \quad \forall \quad k \in x_{\text{ideal}},\ y_{\text{ideal}}, \quad (4)$$

where x_{ideal}, y_{ideal} indicate the projection of the ideal imprint as shown in Fig. 2 top.

Chip Formation:
Since the formation and shape of the machined chip is also of great interest for manufacturing processes[65], we calculate the chip height h_{chip} and volume V_{chip} throughout the simulation. The chip height is simply defined by the z-coordinate of the highest substrate-atom $z_{\max}$. The surface of the substrate gained from the alpha-shape algorithm is used for the evaluation of the chip volume. Only the machined chip in front of the indenter ($x \geqslant x_{\text{P}}$) is taken into account.

$$V_{\text{chip}} = \int_{z=0}^{z_{\max}} \int^{\text{box}} \int^{\text{box}} A^\alpha_{\text{Subs}}(x, y, z)\, \mathrm{d}x\, \mathrm{d}y\, \mathrm{d}z \quad (5)$$

III. RESULTS

We first compare the purely mechanical properties (forces , COF and dislocations) of the dry, weakly adsorbed and strongly adsorbed fluid case followed by the contact zone, chip evolution and surface enlargement characterisation.

A. Mechanical Properties

Forces on the Indenter:
The total normal and total tangential force on the indenter for all three cases (dry, weak wetting and strong wetting) are compared in Fig. 3 (top and centre). The graphs show the entire production phase of the simulations, e. g. the *indentation* in normal direction to the substrate surface, the *scratching* in lateral direction and the *retraction* that removes the indenter in normal direction out of the substrate.

The normal and tangential force on the indenter F_{n} and F_{t} are zero before the first indenter atom reaches z_0 during the indentation (0..150 ps) as after the retraction out of the substrate (750..860 ps). The forces are exactly zero in the dry case (red curves), while the normal and tangential forces in the lubricated cases (green and blue curves) fluctuate around zero during the move through the fluid. As shown in the insets, the fluctuations in the strong adsorbed case are approximately twice as strong as in the weak adsorbed case. This is due to the stronger slip[66,67].

During the normal penetration of the indenter into the substrate (125..300 ps) the normal force rises first in the elastic and then in the plastic regime. The dry case shows two considerable drops of the normal force, which were also reported in[13]. They are due to a diminishment of dislocations at that time. The weakly lubricated case still shows little features of that behaviour, while the strongly lubricated case has a much more constant slope during the indentation. This results from a more constant increase of dislocations in the material in the strongly adsorbed case due to a mechanical coupling of indenter and substrate atoms via fluid molecules. The tangential force in all three simulations increases during the indentation. This is a result from the formation of dislocations and the growth of a chip. As observed for the normal force, the strongly adsorbed fluid has a dampening effect leading to lower fluctuations compared to the other two cases.

At the beginning of the lateral movement, the tangential force F_{t} rises rapidly, due to the chip formation, while the normal force F_{n} decreases, because the contact

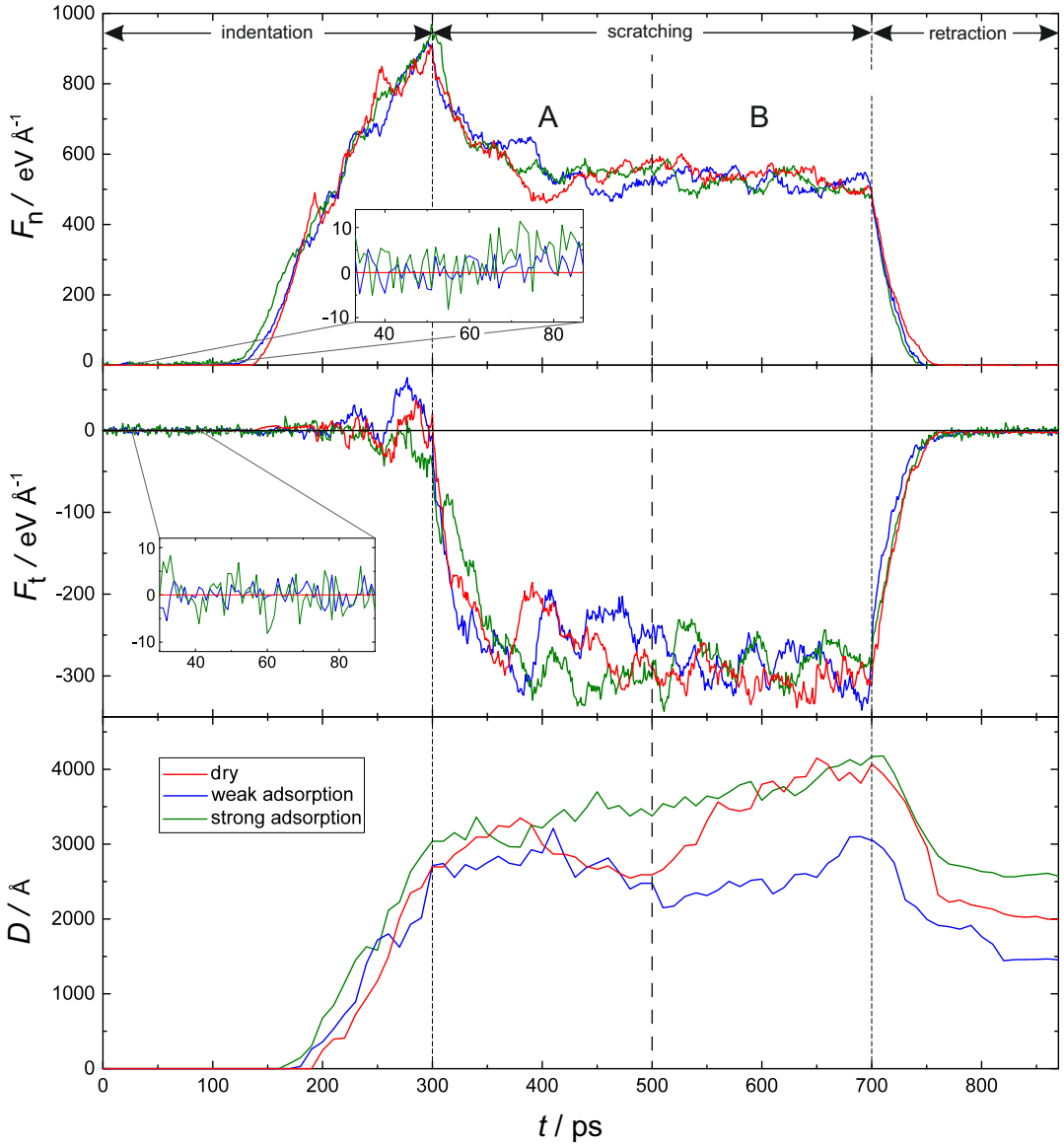

FIG. 3. Normal and tangential forces on the indenter and total dislocation length during the entire simulation (indentation, scratching and retraction). The green and blue lines indicate the lubricated simulations, with strong and weak adsorption, respectively and the solid phases. The red line indicates the dry simulation in vacuum atmosphere.

area of the indenter and the substrate decreases at the beginning of the groove formation. The mechanical behaviour of the scratching phase can be separated in two sub-phases A and B, as indicated in Fig. 3: In a first phase A (300.. appr. 500 ps) the three simulations differ significantly but not systematically. In the second phase B (appr. 500..700 ps) the three simulations lie very close together. The normal and tangential force in that phase behave very similar in all cases.

The normal force in the starting phase A of the scratching does only differ at the very beginning between the three simulations, while the tangential force shows significant differences. The normal force in the strongly adsorbed case reaches a higher maximum around 300 ps than the dry and weakly adsorbed case due to a higher number of trapped fluid molecules. The tangential force in the strong adsorption energy case rises slower, because a significant amount of fluid particles is trapped in the contact zone. These fluid particles act as a spring that gets strained, which leads to a slower increasing tangential force.

During the retraction phase, the normal and tangential force on the indenter decrease back to zero. It can be clearly observed, that the tangential and normal force decrease faster in the two lubricated cases than in the dry case.

During the indentation and scratching process the material is removed from the pit and the groove. This re-

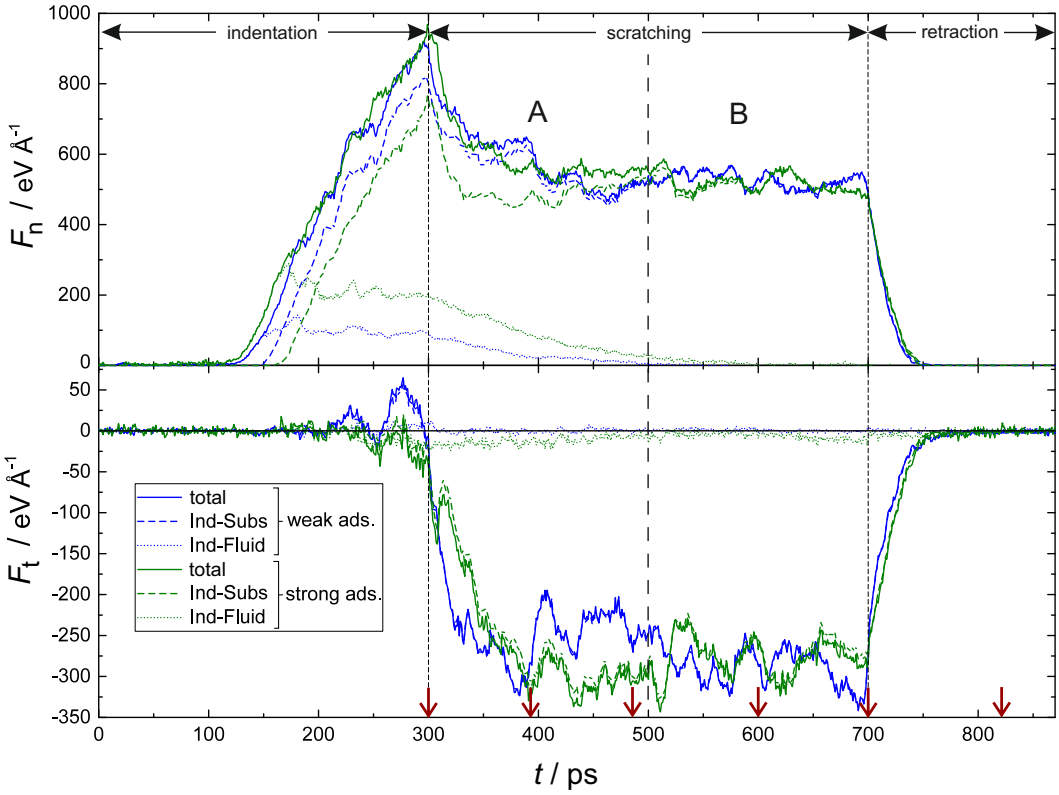

FIG. 4. Normal and tangential forces between the indenter and the substrate (dashed line), between the indenter and the fluid (dotted line) and the total forces on the indenter (solid line) during the entire simulation. The green and blue lines indicate the lubricated simulations, with strong and weak adsorption, respectively. The red arrows indicate the corresponding simulation times for the screenshots shown in fig. 7.

quires strong plastic deformation that shows up in the form of dislocations. The type of dislocations is identified by their Burgers vector b. For bcc Fe there are two important types of dislocations, those with $b = 1/2 < 111 >$ and those with $b =< 100 >$, see Fig. 5. The first one is favoured and dominates since it requires less energy to nucleate and move. The dislocation networks can depend on many factors such as tip geometry, scratching depth. In this study we try to investigate the influence of lubrication on dislocation behaviour.

Fig. 5 shows the dislocation networks at different stages of the scratching process for our three cases. The formation of dislocations is characterized by the formation of long semi-loops of $1/2 < 111 >$ dislocations; these may even detach from the surface and move into the inner of the crystal as prismatic dislocation loops. During scratching the dislocation network changes by addition of newly formed dislocations, but also by the reaction of existing dislocations. The most prominent example of such a reaction is the merging of two $1/2 < 111 >$ dislocations to form a $b =< 100 >$ dislocation. Note that the form of individual dislocations is subject to a high amount of stochastic randomness, caused by thermal fluctuations in the generation process. In view of these fluctuations, the dislocation patterns resulting under the influence of lubrication is not strongly different from that in the dry contact. Thus, for instance, in all cases after removal the tip the dominance of $b = 1/2 < 111 >$ dislocations is reduced and $b =< 100 >$ dislocations become more dominant. This is caused by the high mobility of $b = 1/2 < 111 >$ dislocations that retract back to the surface during the removal of the indenter.

We can analyse the processes of defect formation in the crystal quantitatively by analysing the total dislocation length, see Fig. 3 bottom, during the entire process of indentation, scratching, and tip removal. Clearly, lubrication affects the first nucleation of dislocation in the indentation stage, where plasticity is generated earlier in the two lubricated cases than in the dry case. This appears evident from the fact that the lubricant can transfer forces from the tip to the crystal already before the two solids touch. During scratching, the total dislocation length increases for the case of dry and strong adsorption lubrication, while almost no increment for the case of weak adsorption lubrication. This finding is in line with the snapshots shown in Fig. 5; it seems to be due rather to the more efficient simplification of the reaction network in this case than to the immediate effect of the lubricant. After removal of the tip, the total dislocation length decreases since some dislocation move to the sur-

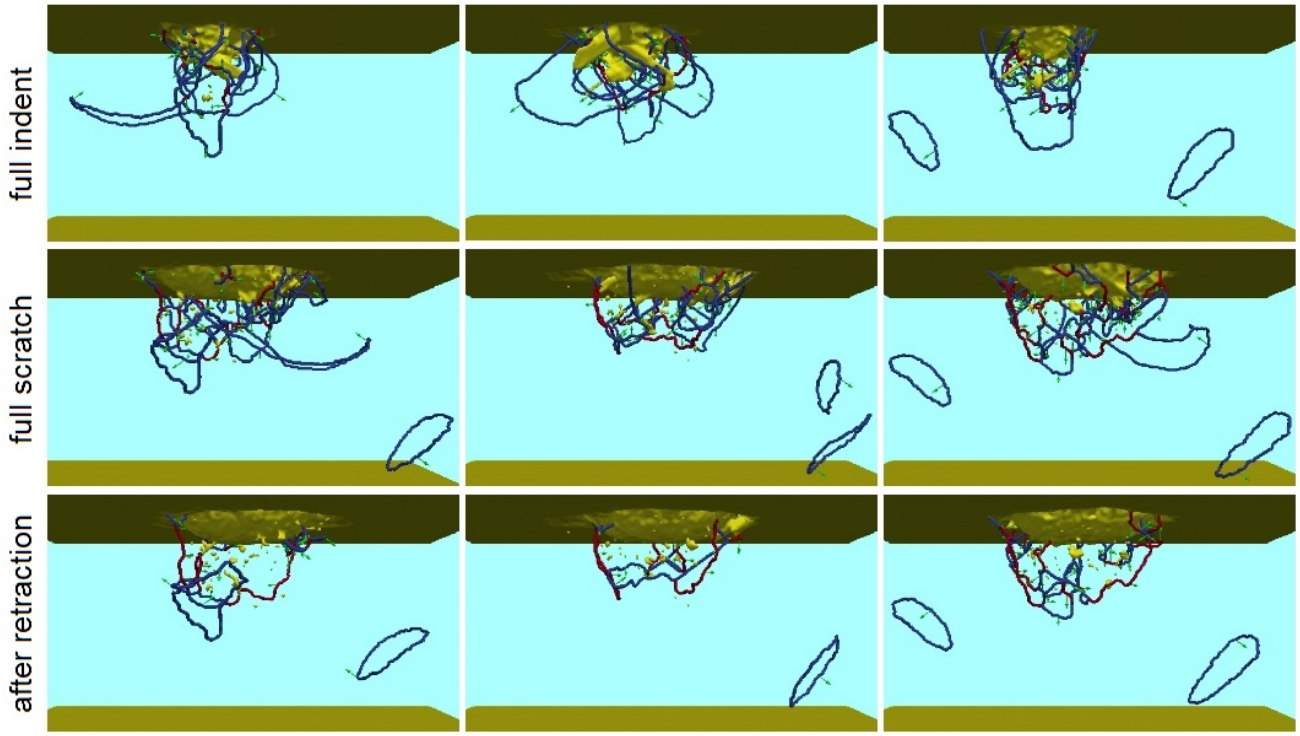

FIG. 5. Evolution of the dislocation network created in the machined crystal after full indentation (top row), at the end of the scratching (centre row) and after the retraction of the tip (bottom row). The case the dry contact is shown in the left column; that of weak adsorption in the middle; and the case of strong adsorption is shown in the right column. Yellow: deformed surface and point defects. Dislocation lines with Burgers vector 1/2 <111> are shown in blue, those with <100> in red. Green arrows indicate direction of the Burgers vector.

face and are annihilated there. We conclude that the main effect of the lubricant on dislocation formation in the material lies in the earlier generation process; during the machining, the effect of the lubricant is hardly visible behind the stochastic fluctuations of the dislocation generation and reaction processes.

Forces Breakdown:
Fig. 4 shows the individual contributions of the forces on the indenter for the two lubricated cases, e. g. the total force between all indenter and substrate atoms (dashed line) and all indenter and fluid atoms (dotted line) in normal and tangential direction. There are three major findings: the indenter-fluid forces have a significant influence during the indentation and the first phase of the scratching A, while the second phase of the scratching B as well as the retraction is hardly affected by the fluid. This agrees with the above mentioned finding, that the three simulations behave very similar from approximately 500 ps because hardly any fluid molecules remain in the contact zone. The second major finding is, that the forces in normal direction are much more affected by the presence of a fluid then the tangential forces throughout the contact process. The third interesting finding is, that the adsorption energy has a significant influence on the different force contributions.

A closer inspection reveals further interesting insights. The total normal force on the indenter rises at the beginning of the indentation only due to the mechanical coupling of the fluid particles between the substrate and the indenter. A stronger mechanical coupling is accompanied by a higher adsorption energy of the fluid, why the normal force in the stronger adsorbing case increases earlier. At the same time when the indenter-fluid force reaches its maximum (appr. 150 ps) the indenter starts penetrating the substrate and the indenter-substrate force increases and becomes quickly dominant. The case with the higher adsorption energy enables a better mechanical coupling, why the indenter-fluid force is about twice as high in that case than in the case with the weak adsorption energy. The number of trapped fluid molecules remains fairly constant, since the indenter-fluid force fluctuates around a constant value during the rest of the indentation. The mechanical coupling of the fluid between the indenter and the substrate leads to a delayed direct contact of the indenter with the fluid for approximately 50 ps. This feature rises with the adsorption energy.

The indenter-fluid normal force decreases during the scratching constantly due to the squeeze-out of the fluid molecules. Moreover the weakly adsorbed fluid case is less influenced by the fluid, such as the indenter-fluid force decreases faster. The indenter-fluid force in the weakly adsorbed fluid case vanishes approximately 100 ps

earlier than the force in the strongly adsorbed fluid case.

The impact of the fluid in tangential direction is on a smaller order of magnitude. In the case with the weak adsorption energy, the indenter-fluid force fluctuates around zero with a magnitude of circa 10 eV/Å and is therefore almost negligible. Nevertheless, the tangential indenter-fluid force in the strongly adsorbed fluid case has a noticeable influence. During the squeeze-out between 300 and 500 ps it decreases to zero and then rises again around 650 ps. This growth is due to the mechanical coupling of the formed chip, the fluid and the indenter, which is not observed in the weakly adsorbed fluid case. This leads already to the assumption, that the chip formation is affected by the presence of a fluid and accordingly the adsorption energy.

Coefficient of friction:

The coefficient of friction (COF) during the scratching phase is shown in Fig. 6 for all three cases (dry, weakly and strongly adsorbed fluid). The inset shows the differences from the two lubricated to the dry reference case. The above mentioned strong similarity between all three simulations in the second half of the scratching phase B becomes very clear by means of the COF. Significant differences can be observed in the first half A. The above mentioned dampening of the tangential force in the strongly adsorbed fluid case leads to a reduced COF with a lower slope in the starting phase (appr. 300..380 ps). The weakly adsorbed fluid case behaves rather similar than the dry case here. In the stationary phase (appr. 380..700 ps) the COF fluctuates around a constant value and other mechanisms dominate the differences. The squeeze-out of the stronger adsorbed fluid particles requires more energy than the weakly adsorbed ones, which leads to an increased COF. Furthermore it becomes clear, that the COF of the strongly adsorbed fluid case has a much smoother trend, than the two other cases. It has a linear trend in the starting phase and then hardly fluctuates around the average value of $\overline{\mu}_{\text{strong.ad.}} = 0.54$ in the stationary phase. The COF average value in the dry case is $\overline{\mu}_{\text{dyr}} = 0.53$, while the weakly adsorbed lubricated case is $\overline{\mu}_{\text{weak.ad.}} = 0.51$. The variance as a measure for the fluctuations is in the stationary phase $\text{var}(\mu_{\text{strong.ad.}}) = 0.028$, which is due to the dampening effect of the trapped fluid particles. The variance of the two other cases is on the other hand $\text{var}(\mu_{\text{weak.ad.}}) = 0.055$ and $\text{var}(\mu_{\text{dry}}) = 0.053$ almost twice as high.

B. Contact Zone and Chip Evolution

Fig. 7 shows screenshots of the contact zone of all three simulations (left: dry, centre: weak adsorption energy, right: strong adsorption energy) at different simulation times. The visualization settings were set as follows: All indenter atoms are visible and opaque, fluid molecules F are visible if they are underneath the unpenetrated substrate surface $z_F < z_0$ and substrate atoms S are visible

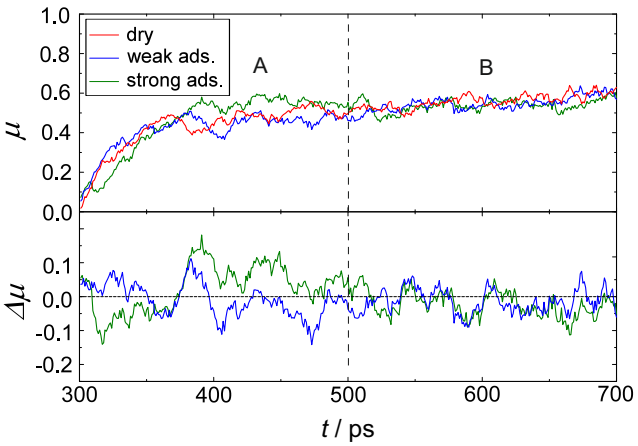

FIG. 6. Coefficient of friction during the scratching process between 300 and 700 ps of the simulation time (top) and the differences of the COF between the lubricated simulations to the dry case (bottom). The red line indicates the dry case, the green and blue lines indicate the lubricated simulations, with strong and weak adsorption interaction respectively.

if they are above the unpenetrated substrate $z_S < z_0$. It illustrates the chip-formation and the squeeze-out during the contact process.

Chip Hight and Chip Volume:

The chip volume and maximum chip height is plotted in Fig. 8, top and centre respectively. The chip volume rises in all three simulations steadily from the beginning of the lateral movement of the indenter as a result of the plastic deformation of the substrate. This growth continues approximately the first 50 ps of the retraction, because the substrate relaxes elastically and thereby lifts the chip. While the chip volume hardly differs between the three cases during the first 200 ps of the scratching, clear discrepancies are observed from there on. The chip volume of the two lubricated cases is increased about 10 % and 20 % respectively compared to the dry case. This is mainly based on a mechanical coupling of the indenter and the chip, not only straight in front of the indenter where the chip is highest but also sideways in y-direction of the spherical indenter, which can also be seen in Fig. 10. Especially in this region the adsorbed fluid molecules widen the indenter from the substrate point of view. The fact that the weakly adsorbed fluid leads to an even higher removal of material than the strongly adsorbed fluid is due to a better diffusion of fluid molecules along the indenter and substrate surface. This leads to a better inflow to the newly formed chip-indenter-fluid contact.

The shape of the tip formed is displayed in Fig. 10. The chip is concentrated on the front part of the groove. This is a simple consequence of the slip systems activated in the single crystal: In bcc crystals, slip occurs on the $\{110\}$ and to a lesser degree also $\{112\}$ planes - in the close-packed $< 111 >$ directions. For our scratch geometry in $[0\ \bar{1}\ \bar{1}]$ direction, hence slip along $[1\ \bar{1}\ \bar{1}]$ will lead to

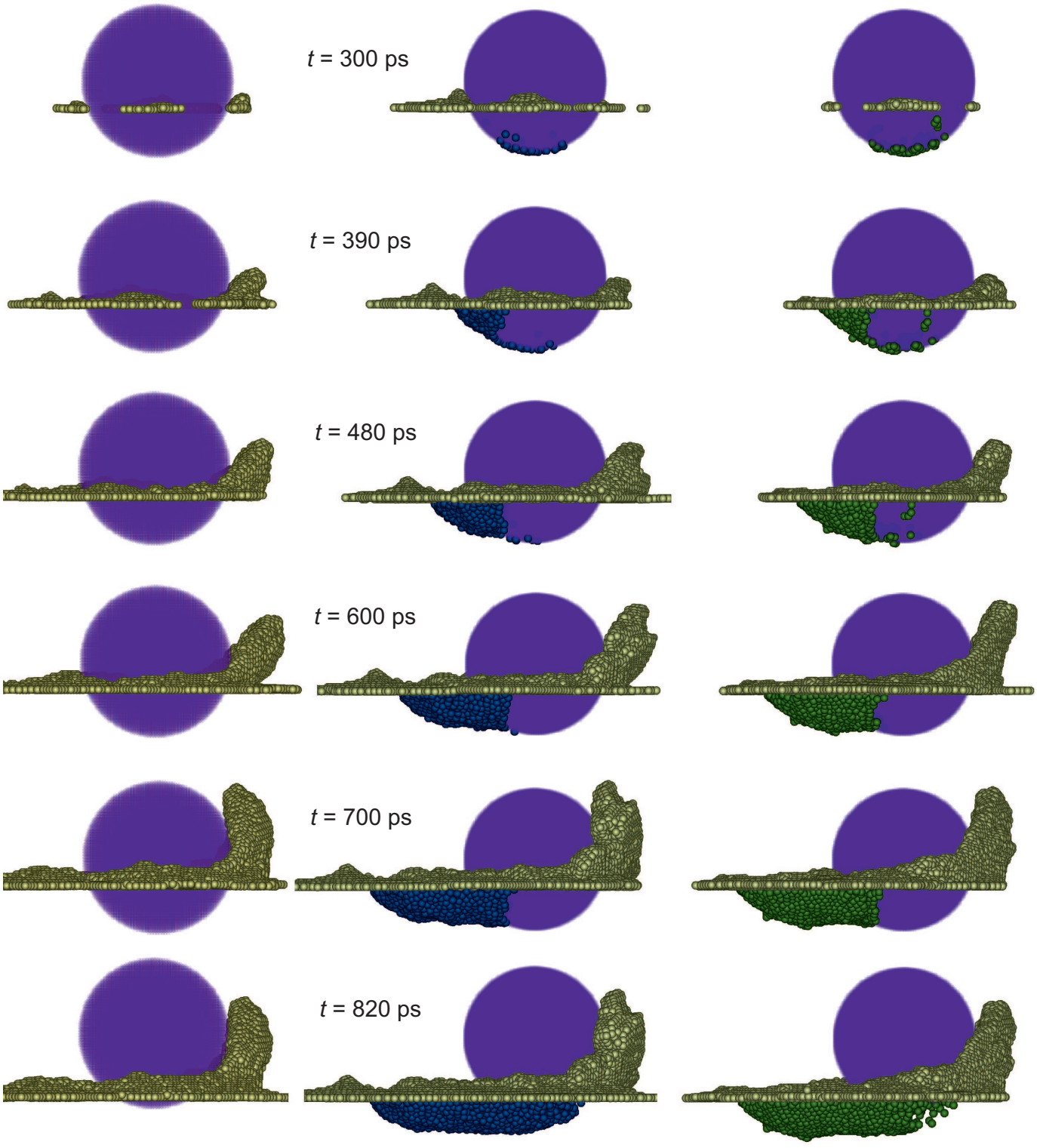

FIG. 7. Screenshots of the contact zone of all three simulations (left: dry; middle: weak adsorption; right: strong adsorption). Each row corresponds to the same simulation time in all three cases as indicated by t. Only the substrate atoms with $z > z_0$ and the fluid molecules with $z < z_0$ are visible for clarity.

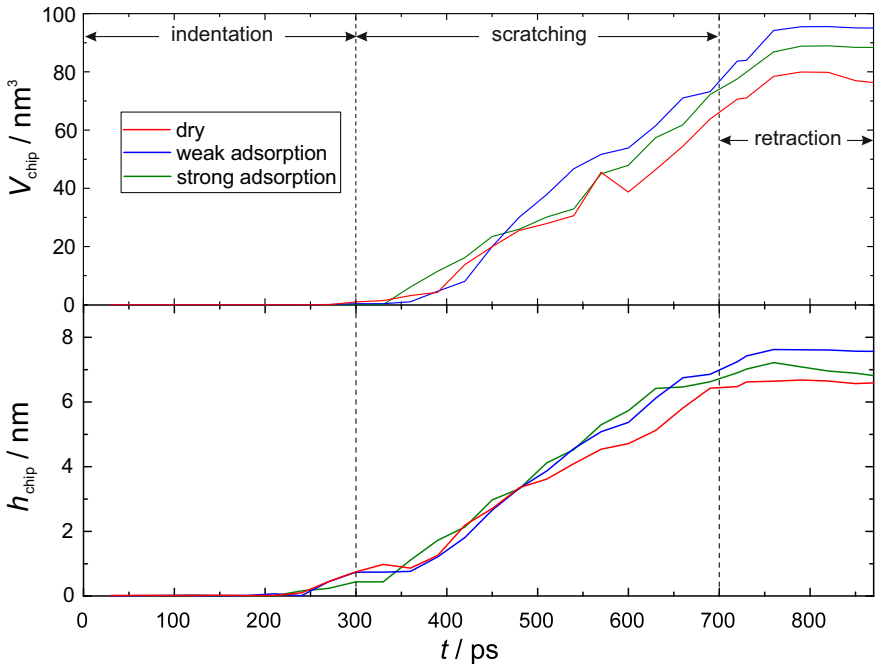

FIG. 8. Characterization of the chip evolution during the simulation (chip volume: top and maximum chip heigth: centre) and the amount of fluid molecules in the gap during the simulation (bottom).

the frontal chip that dominates in Fig. 10. Sideways slip is also generated, but it is not so prominent. This feature is typical of spherical indenters, but may change for other tip forms, see[11]. Most notable for our study is the fact that dry contacts and lubricated contacts lead to the same form of groove and chip.

The same argumentation holds for the maximum chip height. It behaves similar in between the three simulations until approximately 500 ps of the simulation time. From there on h_{chip} for the two lubricated cases lies in average 11 % above the corresponding dry simulation. The centre of the chip is therefore less affected by the presence of a fluid than the flanks of the chip. This becomes also clear from Fig. 10. The two lubricated scenarios differ less in the chip height than the chip volume.

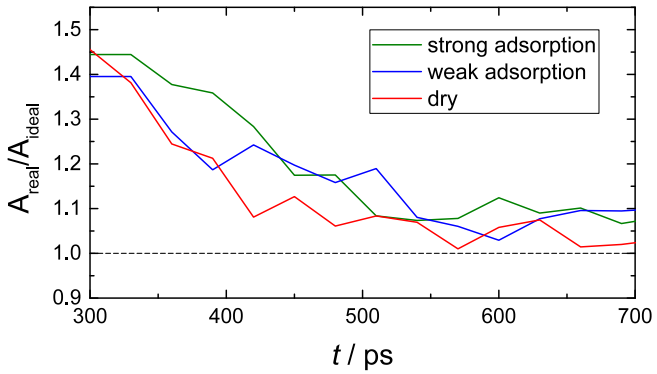

FIG. 9. Surface enlargement of the imprint area, defined as the ratio of the real surface area A_{real} of the imprint in the simulation as sum of finite surface elements and the ideal area A_{ideal}, which is the imprint of a perfect sphere scratched in a substrate.

Surface Enlargement:
The surface enlargement $A_{\mathrm{real}}/A_{\mathrm{ideal}}$ comparing the ideal imprint of a perfect sphere and the real imprint of the atomic surface during the lateral indenter movement is shown in Fig. 9. A constant $A_{\mathrm{real}}/A_{\mathrm{ideal}}(t)$ means, that the surface grows linearly, as the *ideal* reference surface is a linear function of the indenter position $x_{\mathrm{P}}(t)$. The surface enlargement differs strongly from the ideal case ($A_{\mathrm{real}}/A_{\mathrm{ideal}} = 1$) at the beginning (300..400 ps) and converges to a constant value slightly above unity. This is not only a result of the comparison of an atomically resolved surface with an ideal one, but also due to our definition of A_{ideal}, which does not take the atom's size into account, e. g. $\sigma_{\mathrm{ind.\text{-}subs.}}$. But thereby the $A_{\mathrm{real}}/A_{\mathrm{ideal}}$ is independent from the indenter-solid interaction. The decay of $A_{\mathrm{real}}/A_{\mathrm{ideal}}$ during the starting phase of the scratching is a result of the elastic relaxation of the spherical part of the imprint that the indenter leaves behind. The slope of $A_{\mathrm{real}}/A_{\mathrm{ideal}}$ is similar in all three simulations, although the strongly adsorbed fluid case has throughout the scratching process a higher surface enlargement than the dry case. The surface enlargement lies in the strongly adsorbed case in average above the dry one ($\overline{\Delta A_{\mathrm{real}}/A_{\mathrm{ideal}}} = 0.08$). This is due to a stamping of single or clustered fluid molecules into the substrate, during the fluid molecules are squeezed out of the

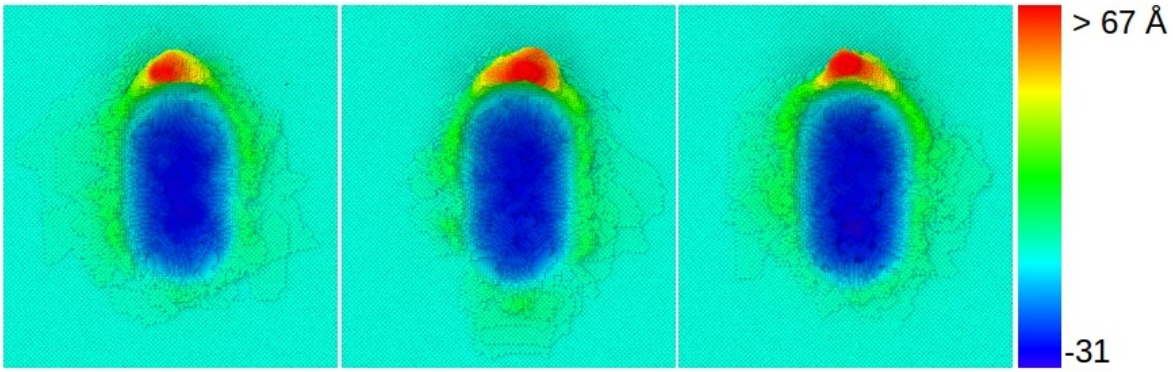

FIG. 10. Top view of the chips formed after scratching and removal of the tip for the case of a dry contact (left), weak adsorption (middle) and strong adsorption (right). Colour denotes height above the original surface plane.

contact zone underneath and asides the indenter. This mechanism was already described by *Bhushan et al.*[68]. The weakly adsorbed fluid case does not differ significantly from the dry case, which is consistent with the observations of the gap volume. The fluid particles are rather individually stamped into the substrate, then leading to a covering liquid film between the two solid bodies at the chosen solid-fluid interaction energies.

Fluid Molecules in the Gap:

The number of trapped fluid molecules in the gap (as defined in fig. 2) during the contact process is shown in Fig. 11 – top. This evaluation is only applied for those timesteps, after the bottom edge of the indenter reached the ground level of the substrate $z_P < z_0$. The amount of fluid molecules rises rapidly during the beginning of the indentation phase. The stronger adsorbed fluid remains longer attached to the indenter and substrate surface resulting in a slower squeeze-out. The amount is even increasing throughout the indentation because the contact area is steadily increasing. The fluid molecules are then squeezed out almost completely between 300..500 ps in the scratching phase, which is in perfect agreement with the indenter-fluid force shown in Fig. 4. The weakly adsorbed fluid on the other side is already partially squeezed out during the indentation and completely pushed out of the gap until circa 520 ps, which is also in good agreement with Fig. 4. The number of trapped fluid molecules is in the strongly adsorbed case in average 3.6 times the amount in the weakly adsorbed case. The squeeze-out duration time is on the other side hardly affected by the adsorption interaction energy.

An other interesting mechanism can be observed during the retraction of the indenter, when the amount of fluid molecules in the gap increases, since the gap itself increases. Liquid fills this increasing gap driven by the pressure difference between the gap and the bulk liquid. As described above, the lateral diffusion rate of adsorbed molecules on a wall increases with an decreasing adsorption interaction energy. Therefore fluid molecules flow faster in the weakly adsorbed case into the growing gap between the indenter and the substrate during the retraction of the indenter, which is clearly visible in the last screenshot in Fig. 7.

Gap Volume:

The development of the gap volume (as defined in Fig. 2) is shown in Fig. 11 – centre. As above, the gap volume evaluation is only done for those timesteps when the bottom of the indenter has reached z_0. The gap volume is calculated as the volume between the indenter surface and the substrate surface calculated by the alpha-shape algorithm that is underneath the substrates unpenetrated surface z_0. This gap volume definition bases on the interaction potential between indenter and substrate atoms and its size parameter $\sigma_{\text{I-S}}$. Therefore it increases linearly during the indentation phase. The gap volume is hardly affected by the presence of a lubrication fluid, since the three curves lie very close together. The reason for this is, that the molecule size σ_{F} has the same order of magnitude as the gap distance $\sigma_{\text{I-S}}$. Thus, the fluid molecules commensurate in the gap in-between the substrate and the indenter. Vice versa fluid molecules only form a mono-layer in the gap at the chosen adsorption energies. Although the difference plot to the dry case in Fig. 11 – bottom reveals, that the strongly adsorbed fluid leads to a slightly increased gap volume (it lies always above the dry case). The weakly adsorbed fluid fluctuates around the dry case.

The gap volume stays fairly constant during the lateral movement of the indenter. The first approximately 50 ps of the indenter's retraction the gap volume stays further constant, because the substrate follows the retraction movement of the indenter due to the substrate's elastic relaxation. After the substrate reaches its final plastically deformed imprint, the gap volume increases again linearly. Due to the inflow of fluid molecules this increase is more distinct in the lubricated cases.

IV. SUMMARY & CONCLUSION

Nano-indentation and -scratching in a Fe (100) surface of a dry and wet contact processes are studied by molecu-

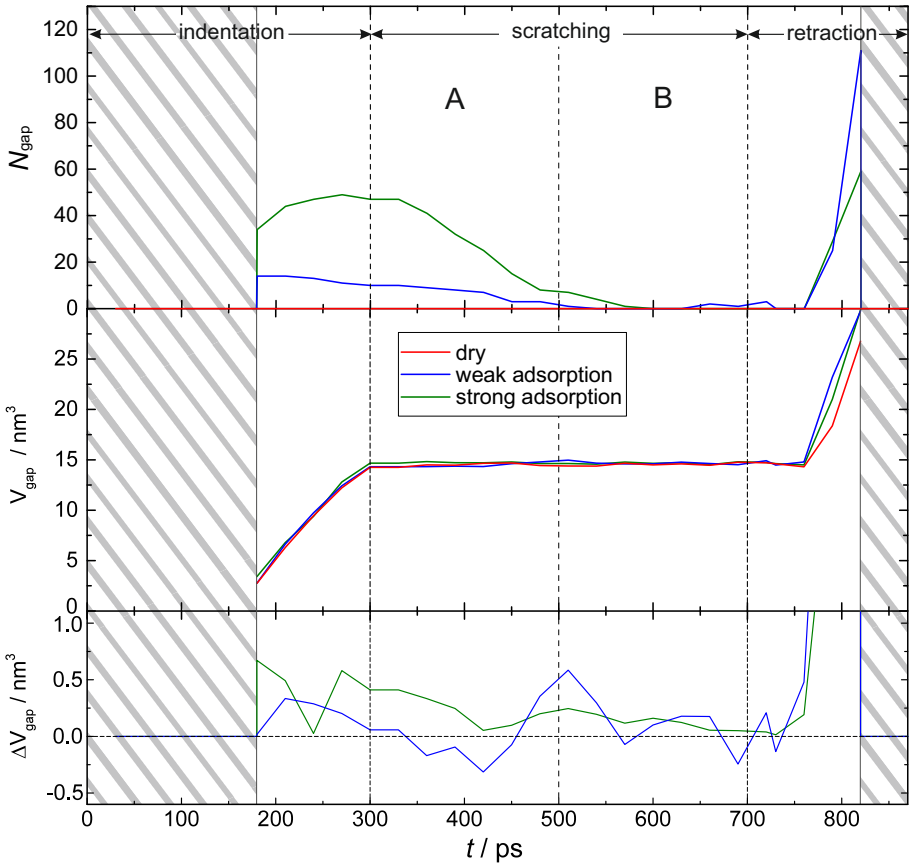

FIG. 11. Top: Trapped fluid molecules in the gap (as defined in Fig. 2) and the gap volume between the indenter and the substrate for $z < z_0$ and $x > x_P$ (bottom).

lar dynamics simulation. Two wet scenarios, differing in the adsorption energy of the fluid molecules on the substrate, are compared with a dry one. We investigate the influence of a lubricant, e. g. methane modelled as a single Lennard-Jones site, and its adsorption energy on the mechanical properties of the process and the squeeze-out. We develop characteristic properties for the evaluation of the effect of a lubricant, e. g. the gap volume, the surface enlargement as a measure for the machined surface quality and the chip volume and height.

While the lubricated case with a relatively weak adsorption energy behaves rather similar to the dry case, considerable differences are found between the a contact process with a stronger adsorbing fluid compared to the dry case.

We find that the fluid has a significant dampening effect, especially in the case of a strong adsorption energy, on most of the examined properties, such as the friction forces, the coefficient of friction, the total dislocation length and the chip formation. While the normal force during the indentation and the chip hight during the scratching in the dry case have distinct turning points, the lubricated cases have a monotonous slope. The dampening due to the presence of the fluid is also considerable in the COF's variance. In the case of the strongly adsorbed fluid the COF fluctuates with half the amplitude than in the dry case. This dampening feature increases significantly with the adsorption energy.

The COF itself is only sightly affected by the presence of a fluid and its adsorption energy. While a strongly adsorbed fluid leads to a slightly increased COF compared to the dry case, a weakly adsorbed fluid decreases the COF. This is mainly a results of a change in the normal force on the indenter, which is about 10 times more affected by the presence of a lubrication fluid than the tangential force.

While high frequent fluctuations with rather small amplitude in the normal and tangential force increase with the adsorption energy during the move of the indenter through a bulk fluid due to a stronger slip (see Fig. 3 – insets), fluctuations are damped during the indentation into the substrate with an increasing adsorption energy vice versa, which is also the reason for the dampening of the COF. This is due to a mechanical coupling between the indenter and the substrate via fluid molecules which balances force peaks. The amount of trapped fluid molecules in the gap correlates almost perfectly with the total normal force between indenter atoms and fluid molecules and increases significantly with the adsorption energy of fluid molecules (see Fig. 4 and 11). Whereat

the squeeze-out time is hardly affected and is around 200 ps of the scratching time. Afterwards the contact zone is dry, e. g. no fluid molecules left in the gap, and thereby the dry and wet simulations practically don't differ.

The chip forming seems independent from the squeeze-out, since the chip evolution does not vary between the three simulations while fluid molecules are trapped in the gap (see Fig. 8). Nonetheless, the chip formation is significantly influenced afterwards by a lubrication fluid which surrounds the chip. Whereat the chip height is less affected by the presence of a fluid than its width. The 10 % and 20 % increase in the chip volume between the strongly and weakly adsorbed fluid case respectively compared to the dry case are in our opinion a results of the inflow of fluid molecules in the constantly newly formed gap between the indenter and the substrate, where material is moved. These fluid molecules broaden the indenter and thereby lead to an increased material removal. This raise of lateral diffusion and mobility with a decreasing adsorption energy becomes also very clear by the fluid inflow during the retraction of the indenter out of the substrate.

Summing up, we find that an increasing adsorption energy has two opposing effects: the fluid particles stick stronger in the gap, since more energy is needed to break the adsorption bonds and squeeze them out of the gap between the relative motion of the indenter and the substrate. A weaker adsorption energy on the other hand favours the lateral diffusion of fluid molecules along the indenter and substrate surface which results in a better inflow to the contact zone.

The gap volume hardly differs between the three simulations, since the size parameter of the fluid molecules has the same order of magnitude as the size parameter of the solid-solid interaction. Hence the fluid or rather the fluid model in combination with the adsorption energy that we employ, does not broaden the gap between the indenter and the substrate. We thereby conclude that the fluid forms a monolayer in the gap in both investigated lubricated cases which can also be seen in Fig. 7.

It would be interesting to investigate the three phase contact line (indenter, fluid, substrate) surrounding the the indenter with respect to the rate of squeezed out fluid molecules out of the gap and the inflow of fluid molecules from the bulk fluid to the contact zone, since this seems to be crucial for the chip formation and surface roughness. An other important question arising from this study is quantification of the statistical uncertainty of the characteristic properties proposed in this work, since the differences are sometimes small and might be in the range of the individual statistical uncertainty.

ACKNOWLEDGEMENT

The authors gratefully acknowledge financial support by the DFG within IRTG 2057 Physical Modelling for Virtual Manufacturing Systems and Processes and CRC 926 Microscale Morphology of Component Surfaces. The simulations were carried out on the HAZELHEN at High Performance Computing Center Stuttgart (HLRS), on the ELWE at Regional University Computing Center Kaiserslautern (RHRK) under the grant TUKL-MSWS as well as on the SUPERMUC at Leibniz Supercomputing Centre (LRZ) Garching within the computing project SPARLAMPE (pr48te). The present research was conducted under the auspices of the Boltzmann-Zuse Society of Computational Molecular Engineering (BZS).

[1] M. Mishra, P. Egberts, R. Bennewitz, and I. Szlufarska, "Friction model for single-asperity elastic-plastic contacts," Physical Review B **86**, 45542 (2012).

[2] T. Junge and J. Molinari, "Molecular dynamics nano-scratching of aluminium: A novel quantitative energy-based analyses method," Procedia IUTAM **3**, 192–204 (2012).

[3] I. Alhafez and H. Urbassek, "Scratching of hcp metals: A molecular-dynamics study," Computational Materials Science **113**, 187–197 (2016).

[4] Y. Gao and H. Urbassek, "Evolution of plasticity in nanometric cutting of fe single crystals," Applied Surface Science **317**, 6–10 (2014).

[5] M. Cho, S. Kim, D. Lim, and H. Jang, "Atomistic scale stick-slip caused by dislocation nucleation and propagation during scratching of a cu substrate with a nanoindenter: A molecular dynamics simulation," Wear **259**, 1392–1399 (2005).

[6] A. Gouldstone, N. Chollacoop, M. Dao, J. Li, A. Minor, and Y. Shen, "Indentation across size scales and disciplines: Recent developments in experimentation and modeling," Acta Materialia **55**, 4015–4039 (2007).

[7] R. Kommanduri and N. Chandrasekaran, "Molecular dynmics simulations of atomic-scale friction," Physical Review B **61**, 14007–14019 (2000).

[8] D. Cui, K. Mylvaganam, L. Zhang, and W. Liu, "Some critical issues for a reliable molecular dynmics simulation of nanomachining," Computational Materials Science **90**, 23–31 (2014).

[9] K. Maekawa and A. Itoh, "Friction and tool wear in nano-scale machining – a molecular dynamics approach," Wear **188**, 115–122 (1995).

[10] R. Kommanduri and L. Raff, "A review on the molecular dynamics simulation of machining at the atomic scale," Proceedings of the Institution of Mechanical Engineers, Part B: Journal of Engineering Manufacture **215**, 1639–1672 (2001).

[11] I. Alhafez, A. Brodyanski, M. Kopnarski, and H. Urbassek, "Influence of tip geometry on nanoscratching," Tribological Letters **65**, 1–13 (2017).

[12] Y. Gao, C. Lu, N. Huynh, G. Michal, H. Zhu, and A. Tieu, "Molecular dynamics simulation of effect of indenter shape on nanoscratching of ni," Wear **267**, 1998–2002 (2009).

[13] Y. Gao, C. Ruestes, and H. Urbassek, "Nanoindentation and nanoscratching of iron: Atomistic simulation of dislocation generation and reactions," Computational Materials Science **90**, 232–240 (2014).

[14] C. Wu, T. Fang, and J. Lin, "Atomic-scale simulations of material behaviors and tribology properties for fcc and bcc metal films," Materials Letters **80**, 59–62 (2012).

[15] Y. Gao, A. Brodyanski, M. Kopnarski, and H. Urbassek, "Nanoscratching of iron: A molecular dynamics study of the influence of surface orientation and scratching direction," Computational Materials Science **103**, 77–89 (2015).

[16] Y. Gao and H. Urbassek, "Scratching of nanocrystalline metals: A molecular dynamics study of fe," Applied Surface Science **389**, 688–695 (2016).

[17] L. Zhang, H. Zhao, Y. Yang, H. Huang, Z. Ma, and M. Shao, "Evaluation of repeated single-point diamond turning on the de-

formation behavior of monochrystalline silicon via molecular dynamics simulation," Applied Physics A (2014).
[18]Y. Li, A. Goyal, A. Chernatynski, J. Jayashanker, M. Kautzky, S. Sinnott, and S. Phillpot, "Nanoindentation of gold and gold alloys by molecular dynamics simulations," Materials Science & Engineering A **651**, 346–357 (2016).
[19]H. Aristizibal, P. Parra, P. Lpez, and E. Restrepo-Parra, "Atomistic-scale simulations of material behaviors and tribology properties for bcc metal films," Chin. Phys. B **25**, 010204 (2016).
[20]J. Israelachvili, *Intermolecular and Surface Forces*, Vol. Third Edition (Academic Press, San Diego, 2011).
[21]I. Szlufarska, M. Chandross, and R. Carpick, "Recent advances in single-asperity nanotribology," Journal of Physics D: Applied Physics **41**, 123001 (2008).
[22]A. Vanossi, N. Manini, M. Urbakh, S. Zapperi, and E. Tosatti, "Modeling friction: From nanoscale to mesoscale," Reviews of Modern Physics **85**, 512–552 (2013).
[23]M. Müser, "Theory and simulation of friction and lubrication," Lect. Notes Phys. **704**, 65–104 (2006).
[24]M. K. Singh, P. Ilg, R. M. Espinosa-Marzal, M. Krger, and N. D. Spencer, "Polymer brushes under shear: Molecular dynamics simulations compared to experiments," Langmuir **31**, 4798–4805 (2015), http://dx.doi.org/10.1021/acs.langmuir.5b00641.
[25]M. K. Singh, P. Ilg, R. M. Espinosa-Marzal, N. D. Spencer, and M. Krger, "Influence of chain stiffness, grafting density and normal load on the tribological and structural behavior of polymer brushes: A nonequilibrium-molecular-dynamics study," Polymers **8**, 1–18 (2016).
[26]X. Zheng, H. Zhu, A. Tieu, and B. Kosasih, "A molecular dynamics simulation of 3d rough lubricated contact," Tribology International **67**, 217–221 (2013).
[27]X. Zheng, H. Zhu, B. Kosasih, and A. Tieu, "A molecular dynamics simulation of boundary lubrication: The effect of n-alkanes chain length and normal load," Wear **301**, 62–69 (2013).
[28]I. Sivebaek and B. Persson, "The effect of surface nanocorrugation on the squeeze-out of molecular thin hydrocarbon films between curved surfaces with long range elasticity," Nanotechnology **27**, 445401 (2016).
[29]J. Ren, J. Zhao, Z. Dong, and P. Liu, "Molecular dynamics study on the mechanism of afm-based nanoscratching process with water-layer lubrication," Applied Surface Science **346**, 84–98 (2015).
[30]R. Chen, M. Liang, J. Luo, H. Lei, D. Guo, and X. Hu, "Comparison of surface damage under the dry and wet impact: Molecular dynamics simulation," Applied Surface Science **258**, 1756–1761 (2011).
[31]C. Tang and L. Zhang, "A molecular dynamics analysis of the mechanical effect of water on the deformation of silicon monocrystals subjected to nano-indentation," Nanotechnology **16**, 15–20 (2005).
[32]Y. Chen, H. Han, F. Fang, and X. Hu, "Md simulation of nanometric cutting of copper with and without water lubrication," Science China **57**, 1154–1159 (2014).
[33]M. Chandross, C. Lorenz, M. Stevens, and G. Grest, "Simulations of nanotribology with realistic probe tip models," Langmuir **24**, 1240–1246 (2008).
[34]R. An, L. Huang, Y. Long, B. Kalanyan, X. Lu, and K. Gubbins, "Liquid-soild nanofriction and interfacial wetting," Langmuir **32**, 743–750 (2015).
[35]J. Shi, Y. Zhang, K. Sun, and L. Fang, "Effect of water film on the plastic deformation of monocrystalline copper," RSC Advances **6**, 96824–96831 (2016).
[36]Y. Jeng, P. Tsai, and Y. Liu, "Adsorbed multilayer effects on the mechanical properties in nanometer indentation depth," Materials Research Bulletin **44**, 1995–1999 (2009).
[37]W. Lee, S. Ju, and C. Cheng, "A molecular dynamics study of nanoindentation on a methyl methacrylate ultrathin film on a au (111) substrate: Interface and thickness effects," Langmuir **24**, 13440–13449 (2008).
[38]F. Yang, R. Carpick, and D. Srolovitz, "Mechanics of contact, adhesion and failure of metallic nanoasperites in the presence of adsorbates: Toward conductive contact design," ACS Nano **11**, 490–500 (2017).
[39]B. Shiari, R. Miller, and D. Klug, "Multiscale simulation of material removal processes at the nanoscale," Journal of the Mechanics and Physics of Solids **55**, 2384–2405 (2007).
[40]C. Greiner, J. Felts, Z. Dai, and R. King, W.P. andCarpick, "Controlling nanoscale friction through th competition between capillary adsorption and thermally activated sliding," ACSNano **6**, 4305–4313 (2012).
[41]S. O'Shea, N. Gosvami, L. Lim, and W. Hofbauer, "Liquid atomic force microscopy: Solvation forces, molecular order, and squeeze-out," Japanese Journal of Applied Physics **49**, 08LA01 (2010).
[42]E. Cihan, S. Ipek, and M. Baykara, "Structural lubricity under ambient conditions," Nature Communications **7**, 12055 (2016).
[43]L. Dai, V. Sorkin, and Y. Zhang, "Effect of surface chemistry on the mechanics and governing laws of friction and wear," ACS Applied Materials & Interfaces **8**, 8765–8772 (2016).
[44]U. Tartaglino, I. Sivebaek, B. Persson, and E. Tosatti, "Impact of molecular structure on the lubrication squeeze-out between curved surfaces with long range elasticity," The Journal of Chemical Physics **125**, 014704 (2006).
[45]R. Rentsch and I. Inasaki, "Effects of fluids on the surface generation in material removal processes - molecular dynamics simulation -," Annals of the CIRP **55**, 601604 (2006).
[46]M. Lautenschläger, S. Stephan, H. Urbassek, B. Kirsch, J. Aurich, M. Horsch, and H. Hasse, "Effects of lubrication on the friction in nanometric machining processes: A molecular dynamics approach," ??? (2017).
[47]M. Lautenschläger, S. Stephan, M. Horsch, B. Kirsch, J. Aurich, and H. Hasse, "Effects of lubrication on the friction and heat transfer in machining processes on the nanoscale: A molecular dynamics approach," Procedia CRIP (2017).
[48]S. Becker, H. Urbassek, M. Horsch, and H. Hasse, "Contact angle of sessile drops in lennard-jones systems," Langmuir **30**, 13606–13614 (2014).
[49]S. Banerjee, S. Naha, and I. K. Puri, "Molecular simulation of the carbon nanotube growth mode during catalytic synthesis," Applied Physics Letters **92**, 233121 (2008), http://dx.doi.org/10.1063/1.2945798.
[50]M. I. Mendelev, S. Han, D. J. Srolovitz, G. J. Ackland, D. Y. Sun, and M. Asta, "Development of new interatomic potentials appropriate for crystalline and liquid iron," Philosophical Magazine **83**, 3977–3994 (2003), http://dx.doi.org/10.1080/14786430310001613264.
[51]C. Chen, P. Depa, J. K. Maranas, and V. G. Sakai, "Comparison of explicit atom, united atom, and coarse-grained simulations of poly(methyl methacrylate)," The Journal of Chemical Physics **128**, 124906 (2008), http://dx.doi.org/10.1063/1.2833545.
[52]M. Allen and D. Tildesley, *Computer Simulations of Liquids* (Oxford, 2009).
[53]J. Vrabec, G. K. Kedia, G. Fuchs, and H. Hasse, "Comprehensive study of the vapour-liquid coexistence of the truncated and shifted Lennard-Jones fluid including planar and spherical interface properties," Molecular Physics **104**, 1509 (2006).
[54]U. Setzmann and W. Wagner, "A new equation of state and tables of thermodynamic properties for methane covering the range from the melting line to 625 k at pressures up to 100 mpa," Journal of Physical and Chemical Reference Data **20**, 1061–1155 (1991), http://dx.doi.org/10.1063/1.555898.
[55]S. Becker, R. Merz, H. Hasse, and M. Kopnarski, "Solvent cleaning and wettability of technical steel and titanium surfaces," Adsorption Science & Technology **34**, 261–274 (2016), http://dx.doi.org/10.1177/0263617416645110.
[56]K. Mittal, *Surface Contamination*, edited by K. Mittal (Springer, New York, 1979).
[57]S. Plimpton, "Fast parallel algorithms for short-range molecular dynamics," J. Comp. Phys. **117**, 1–19 (1995).

[58] A. Stukowski and K. Albe, "Extracting dislocations and non-dislocation crystal defects from atomistic simulation data," Modelling and Simulation in Materials Science and Engineering **18**, 085001 (2010).
[59] A. Henderson, "Paraview guide, a parallel visualization application," Kitware Inc. (2007), http://www.paraview.org.
[60] H. Childs, E. Brugger, B. Whitlock, J. Meredith, S. Ahern, D. Pugmire, K. Biagas, M. Miller, C. Harrison, G. H. Weber, H. Krishnan, T. Fogal, A. Sanderson, C. Garth, E. W. Bethel, D. Camp, O. Rübel, M. Durant, J. M. Favre, and P. Navrátil, "VisIt: An End-User Tool For Visualizing and Analyzing Very Large Data," in *High Performance Visualization–Enabling Extreme-Scale Scientific Insight* (2012) pp. 357–372.
[61] A. Stukowski, "Visualization and analysis of atomistic simulation data with ovito - the open visualization tool," Modelling and Simulation in Materials Science and Engineering **18**, 015012 (2010), http://www.ovito.org/.
[62] E. Brinksmeier, J. Aurich, E. Goveka, C. Heinzel, H. Hoffmeister, F. Klocke, J. Peters, R. Rentsch, D. Stephenson, E. Uhlmann, K. Weinert, and M. Wittmann, "Advances in modeling and simulation of grunding processes," Annals of the CIRP **55**, 667–696 (2006).
[63] H. Edelsbrunner, D. Kirkpatrick, and R. Seidel, "On the shape of a set of points in the plane," IEEE Transactions on Information Theory **29**, 551–559 (1983).
[64] E. Brinksmeier, C. Heinzel, and M. Wittmann, "Friction, cooling and lubrication in grinding," Annals of the ClRP **48**, 581–598 (1999).
[65] R. Snoeys, J. Peters, and A. Decneut, "The mean undeformed chip thickness as a basic parameter in grinding," Annals of the CIRP **32**, 227–237 (1974).
[66] P. A. Thompson, "A general boundary condition for liquid flow at solid surfaces," nature **389**, 360–362 (1997).
[67] X. Yong and L. T. Zhang, "Slip in nanoscale shear flow: Mechanisms of interfacial friction," Microfluidics and Nanofluidics **14**, 299–308 (2013).
[68] B. Bhushan, J. Israelachvili, and U. Landman, "Nanotribology: Friction, wear and lubrication at the atomic scale," Nature **374**, 607–616 (1995).